




# Integrated conversion and photodetection of virtual photons in an ultrastrongly coupled superconducting quantum circuit

Luigi Giannelli<sup>1,2,3,a</sup> , Giorgio Anfuso<sup>2</sup>, Miroslav Grajcar<sup>4</sup>, Gheorghe Sorin Paraoanu<sup>5</sup>, Elisabetta Paladino<sup>1,2,3</sup>, and Giuseppe Falci<sup>1,2,3</sup>

<sup>1</sup> CNR-IMM, UoS Università, 95123 Catania, Italy

<sup>2</sup> Dipartimento di Fisica e Astronomia “Ettore Majorana”, Università di Catania, Via S. Sofia 64, 95123 Catania, Italy

<sup>3</sup> INFN Sez. Catania, 95123 Catania, Italy

<sup>4</sup> Department of Experimental Physics, Comenius University, 84248 Bratislava, Slovakia

<sup>5</sup> QTF Centre of Excellence, Department of Applied Physics, Aalto University, P.O. Box 15100, 00076 Aalto, Finland

Received 6 June 2023 / Accepted 22 August 2023 / Published online 8 September 2023

© The Author(s) 2023

**Abstract** The ground state of an artificial atom ultrastrongly coupled to quantized modes is entangled and contains an arbitrary number of virtual photons. The problem of their detection has been raised since the very birth of the field, but despite the theoretical efforts still awaits experimental demonstration. Recently, experimental problems have been addressed in detail showing that they can be overcome by combining an unconventional design of the artificial atom with advanced coherent control. In this work, we study a simple scheme of control-integrated continuous measurement, which makes remarkably favorable the tradeoff between measurement efficiency and backaction showing that the unambiguous detection of virtual photons can be achieved within state-of-the-art quantum technologies.

## 1 Introduction

Advancement of fabrication technologies has allowed producing solid-state systems which exhibit the physics of atoms ultrastrongly coupled (USC) to quantized modes [1–4]. In these systems, the coupling constant  $g$  between the artificial atom (AA) and the mode is comparable or even larger than the bare excitation frequencies  $\epsilon$  and  $\omega_c$  of the AA and of the mode. This regime has been achieved on several different platforms [2, 3], semiconductors [5–7] and superconductors [8–10] being the most promising for applications.

In the USC regime, nonperturbative physics is predicted to emerge [2, 3] which is undetectable in the standard strong-coupling regime of quantum optics [11, 12]. Higher-order antiresonant terms in the Hamiltonian break the conservation of the number of excitations this occurrence being at the heart of most of the phenomenology USC is expected to exhibit. A striking feature is that eigenstates are highly entangled, and in particular the ground-state  $|\Phi\rangle$  contains virtual photons (VP). The simplest instance is the two-level quantum Rabi model [13, 14]

$$H_R = \epsilon |e\rangle\langle e| + g(a^\dagger + a)(|g\rangle\langle e| + |e\rangle\langle g|) + \omega_c a^\dagger a \quad (1)$$

where  $\{|g\rangle, |e\rangle\}$  are the eigenstates of a two-level atom and  $a$  ( $a^\dagger$ ) are the annihilation (creation) operators of a quantized harmonic mode. The ground state has the form

$$|\Phi\rangle = \sum_{n=0}^{\infty} (|2n g\rangle\langle 2n g|\Phi\rangle + |2n + 1 e\rangle\langle 2n + 1 e|\Phi\rangle) \quad (2)$$

$\{|n\rangle\}$  being the number eigenstates of the mode [2, 3]. It is seen that  $|\Phi\rangle$  contains an even number  $\hat{N} = \hat{n} + |e\rangle\langle e|$  of excitations while in the absence of USC the ground state is  $|0g\rangle$  thus it is factorized and it does not contain VPs. The question of how to detect ground-state VPs in USC systems has been posed since the birth of the field [1]. They cannot be probed by standard photodetection because the USC vacuum  $|\Phi\rangle$  cannot radiate [15], thus VPs must be converted to real excitations which are then detectable. Early theoretical proposals of VP detection leverage time-dependent coupling constants as in the dynamical Casimir effect [16–18] but require modulation of quantum hardware at subnanosecond times which is still unavailable. Another

<sup>a</sup> e-mail: [luigi.giannelli@dfa.unict.it](mailto:luigi.giannelli@dfa.unict.it) (corresponding author)

class of proposals formulated in the last decade [19–23] introduces an additional lower energy AA level  $|u\rangle$  not coupled to the mode (see Fig. 1a) making  $|\Phi\rangle$  a false vacuum which can undergo radiative decay. This option also poses several experimental challenges, from the low yield of detectable photons to the fact that conventional quantum hardware does not ensure that the conversion is faithful, i.e., that output photons are really produced due solely to USC [23]. For these reasons, despite the huge theoretical effort, detection of VPs still awaits demonstration. In a recent work [24], it has been shown that the above experimental problems can be overcome. Efficient, faithful and selective conversion of VPs to real ones can be achieved by combining an unconventional superconducting multilevel AA design [25–27], with coherent amplification of the conversion of ground-state VPs by advanced control [21] and a tailored measurement protocol.

In this work, we discuss a toy model of integrated protocol combining VP conversion by STIRAP [24] with photodetection by continuous measurement of the mode [28]. In particular, we consider decay into a transmission line coupled to the mode during the whole protocol, which is the simplest experimental option. A detectable signal is obtained if the decay rate  $\kappa$  of the mode is large enough which however, determines a backaction of the continuous measurement inducing decoherence which may affect the efficiency of the coherently amplified conversion. Our results show that STIRAP is resilient to this backaction making favorable the tradeoff of the integrated protocol with a continuous measurement.

## 2 Model

We illustrate VPs conversion/detection considering the Hamiltonian of a three-level AA coupled to the mode (see Fig. 1a)

$$H = H_R - \epsilon' \mathbb{1}_{osc} \otimes |u\rangle\langle u| + \omega_c a^\dagger a \otimes |u\rangle\langle u|. \quad (3)$$

Hamiltonian (3) describes a three-level AA with the two excited states  $|g\rangle$  and  $|e\rangle$  ultrastrongly coupled to the mode, as described in Eq. (1), and the ground state  $|u\rangle$  uncoupled. It is a three-level approximation of the multilevel Hamiltonian described in ref. [24], which is implemented by a fluxonium-like superconducting AA galvanically coupled to a mode also implemented by a superconducting LC resonator. Parameters for the lumped elements of this quantum circuit have been found such that coupling of  $|u\rangle$  to the mode is very small, thus guaranteeing that only VPs are converted in real photons. For instance, the first level splitting  $\epsilon' > 0$  of the “uncoupled” state  $|u\rangle$  is much larger than  $\omega_c = \epsilon$ , the latter being the second atomic splitting. For a detailed discussion, we refer to ref. [24]. The eigenstates of  $H$  are classified in two sets (see Fig. 1a), namely the factorized states  $\{|n\rangle \otimes |u\rangle\}$  with

energies  $-\epsilon' + n\omega_c$ , and the entangled Rabi-like eigenstates  $\{|\Phi_l\rangle\}$  of  $H_R$ , with eigenvalues  $E_l$ .

### 2.1 Conversion of VPs

Conversion of VPs employs a STIRAP protocol [29] where the system is driven by a two-tone field  $W(t) = \mathcal{W}_s(t) \cos \omega_s t + \mathcal{W}_p(t) \cos \omega_p t$  mainly coupled with the  $u - g$  transition of the AA. We take the field resonant with the two relevant transitions  $\omega_p \approx E_0 + \epsilon'$  and  $\omega_s \approx E_0 + \epsilon' - 2\omega_c$ . Standard approximations yield the  $\Lambda$  driving configuration [30] of Fig. 1a described in a rotating frame by the control Hamiltonian [21]

$$\tilde{H}_C(t) = \frac{\Omega_p(t)}{2} |0u\rangle\langle\Phi| + \frac{\Omega_s(t)}{2} |2u\rangle\langle\Phi| + \text{h.c.}, \quad (4)$$

where the Rabi amplitudes  $\Omega_p(t) = \mathcal{W}_p(t) \gamma_{ug} \langle 0g|\Phi\rangle$  and  $\Omega_s(t) = \mathcal{W}_s(t) \gamma_{ug} \langle 2g|\Phi\rangle$  depend on the matrix element  $\gamma_{ug} := \langle u|\hat{\gamma}|g\rangle$  of the AA “dipole” operator [24]. Operating the “counterintuitive” pulse sequence [29]  $\Omega_{p/s}(t) = F[(t \mp \tau)/T_W]$  with  $\tau > 0$ , the Stokes pulse is shined before the pump pulse (see Fig. 1b, top panel). Using for instance Gaussian pulses of width  $T_W$ , coherent population transfer  $|0u\rangle \rightarrow |2u\rangle$  occurs with  $\sim 100\%$  probability provided the “global adiabaticity” condition  $\max_t [\Omega_s(t)] T_W \gtrsim 10$  [31, 32] is met [21]. Population transfer may occur only if  $\Omega_s(t) \propto \langle 2g|\Phi\rangle \neq 0$ , thus it provides a “smoking gun” of the presence of

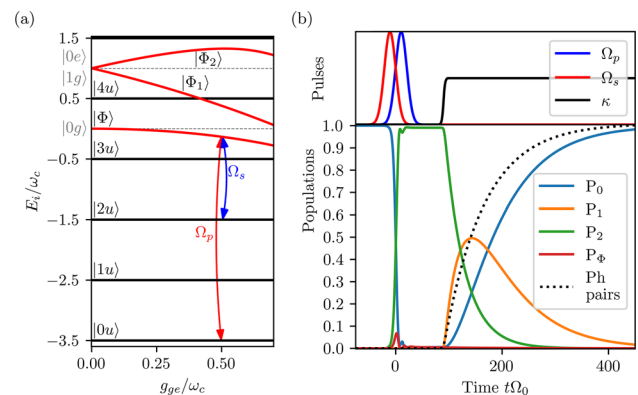


**Fig. 1** **a** Spectrum of the multilevel AA extended Rabi model with the additional uncoupled state  $|u\rangle$ , Eq. (3), as a function of  $g$  and the scheme of the Lambda configuration used to drive the system, Eq. (4). **b** Top panel: Gaussian pulses  $\Omega_{s/p}(t)$  in the counterintuitive sequence for the coherent amplification protocol and the sigmoid function  $\kappa(t - t_{sm})$  mimicking a switchable meter. Bottom panel: population histories; for  $t < t_{sm}$  population transfer  $|0u\rangle \rightarrow |2u\rangle$  by STIRAP is completed; for  $t > t_{sm}$  the mode decays, emitting two photons and resetting the system to the initial state. Parameters are given in Table 1. The protocol starts at  $\Omega_0 t_i = -75$  and ends at  $\Omega_0 t_f = 450$ , the meter is switched on at  $\Omega_0 t_{sm} = 90$ . We used the shorthand notation for the populations  $P_n := \langle n, u|\rho(t)|n, u\rangle$  for  $n = 0, 1, 2$  and  $P_\Phi := \langle \Phi|\rho(t)|\Phi\rangle$ , where  $\rho(t)$  is the density matrix of the system

VPs in the ground state. In the target state  $|2u\rangle$ , two real photons are present, witnessing the presence of the two-VP component in  $|\Phi\rangle$ . Therefore, this protocol guarantees 100% conversion efficiency, thanks to coherence. In this case, the dynamics is restricted to the subspace spanned by the eigenstates  $\{|0u\rangle, |2u\rangle, |\Phi\rangle\}$ . Population histories are shown in the lower panel of Fig. 1b, population transfer by STIRAP occurring in the first part of the protocol. As shown in Ref. [24], the nearly ideal scenario described in this section can be implemented also in the USC regime by state-of-the-art superconducting quantum technologies in an unconventional design of the quantum circuit, and using superinductors [25–27] and advanced control at microwave frequencies. Control based on STIRAP has been proposed [33–36] and demonstrated [37, 38] in standard superconducting quantum devices.

## 2.2 Toy model for photodetection

Ideally, once the population has been transferred in  $|2u\rangle$ , the converted VP pair can be detected. For oscillators with quality factor  $Q \gtrsim 10^4$ , the population of the mode remains large enough [39] to allow photons to be detected (and even counted) by single-shot non-demolition measurements performed by a quantum probe coupled dispersively to the mode [40, 41]. A much simpler procedure is a continuous measurement [28] which uses radiative decay of converted VPs with a rate  $\kappa$  into a transmission line. In this case, a key advantage is that the initial state is faithfully prepared by simply letting the system relax [42] due to photodetection. Thus, the protocol can be repeated over and over yielding a detectable signal if  $\kappa$  is large enough.

Since the oscillator selection rules prevent direct  $|2u\rangle \rightarrow |0u\rangle$  decay, photodetection involves the sequential decay of the mode  $|2u\rangle \rightarrow |1u\rangle \rightarrow |0u\rangle$ . Therefore, we formulate a minimal model restricting the analysis to the four-dimensional Hilbert space spanned by  $\{|0u\rangle, |1u\rangle, |2u\rangle, |\Phi\rangle\}$ . In Fig. 1b, we show the population histories with an oscillator decay rate  $\kappa(t)$  turned on after the completion of STIRAP. Photons in  $|2u\rangle$  first decay to  $|1u\rangle$  and then to  $|0u\rangle$  at each step a photon being emitted into the transmission line. A minimal model of decay is described by a Lindblad equation with Lindbladian given by

$$\mathcal{L}_\kappa = \kappa \mathcal{D}[\hat{a}] + \kappa e^{-\beta\omega_c} \mathcal{D}[\hat{a}^\dagger] \quad (5)$$

where the dissipator is defined as  $\mathcal{D}[\hat{A}]\hat{\rho} = \hat{A}\hat{\rho}\hat{A}^\dagger - \frac{1}{2}(\hat{A}^\dagger\hat{A}\hat{\rho} + \hat{\rho}\hat{A}^\dagger\hat{A})$  and  $\hat{\rho}$  is the density matrix of the system. The first term describes emission with decay rate  $\kappa$  and the second describes absorption whose rate has been written making the phenomenological assumption that detailed balance at thermal equilibrium,  $\beta = 1/(k_B T)$ , can be used also for the driven system.

We point out that some care is required to guarantee a physically consistent picture of photon decay. We now briefly describe how to interpret Eq. (5) to obtain the minimal model of photodetection. The key point is

that the operator  $\hat{a}$  must be defined such to avoid photon annihilation in the Rabi ground state  $|\Phi\rangle$  otherwise we could have photon emission even in the absence of the level  $|u\rangle$ , which is unphysical. The complete theory requires using “dressed” field operators, say  $\hat{a} \rightarrow \hat{A}$  [3]. In our case, this brings a simplification since the new operators are such that  $\hat{A}|\Phi\rangle = 0$  and they reduce to  $\hat{a}$  when acting on  $|nu\rangle$ . Since truncation to the four-level space also implies that  $\hat{A}^\dagger|\Phi\rangle = 0$ , we simply have to use a projected version of the bare jump operators acting only on states  $|nu\rangle$ . This provides the correct minimal description of both decoherence and photodetection.

The measured quantity is the extra current of photons emitted into the transmission line defined as

$$j_T = \kappa [\overline{\langle \hat{a}^\dagger(t)\hat{a}(t) \rangle} - \langle \hat{a}^\dagger\hat{a} \rangle_{th}] \quad (6)$$

where the first term is the average total current for the driven system

$$\overline{\langle \hat{a}^\dagger(t)\hat{a}(t) \rangle} = \frac{1}{t_M} \int_0^{t_M} dt \langle \hat{a}^\dagger(t)\hat{a}(t) \rangle$$

where  $t_M$  is the duration of the whole integrated conversion and measurement protocol and the second term is the equilibrium thermal current in the undriven system. Figure 1b also shows the number of emitted photon pairs (black dashed line) in a cycle at zero temperature when the thermal current is also zero. The parameters used are such that the VPs conversion is complete and the system is reset to the initial state  $|0u\rangle$ .

### 2.2.1 Atomic decay

In principle, atomic decay is not relevant in the ideal protocol since in STIRAP the intermediate state  $|\Phi\rangle$  is expected not to be populated (see Fig. 1b). However, we will see that AA decay plays a role in the integrated conversion/measurement protocol (see Fig. 2a). Thus, we take into account it in the Lindblad formalism by introducing two dissipators with jump operators  $|0, u\rangle\langle\Phi|$  and  $|2u\rangle\langle\Phi|$ . Nonradiative decay rates could be explicitly calculated by the Fermi Golden Rule if the atomic environment were specified. Even in the absence of detailed information, we know that the rates  $|\Phi\rangle \rightarrow |nu\rangle$  are proportional to the square of the matrix elements  $\langle nu | [\mathbb{1}_{osc} \otimes |u\rangle\langle g|] |\Phi\rangle = \langle ng | \Phi \rangle$ . Thus, once again we express them in terms of a single parameter  $\gamma$  as

$$\gamma_{0\Phi} = |\langle 0g | \Phi \rangle|^2 \gamma; \quad \gamma_{2\Phi} = |\langle 2g | \Phi \rangle|^2 \gamma.$$

The excitation rates at equilibrium are written assuming again that detailed balance holds and finally, we obtain the Lindbladian

**Table 1** Parameters used in the simulations and corresponding physical values for the superconducting flux-based architecture including a superconducting junction with Josephson energy  $E_J/(2\pi) = 10$  GHz considered in Ref. [24], where an extended Rabi model was studied with coupling constant  $g/\omega_c = 0.5$  yielding squared matrix elements  $|\langle 0|g|\Phi\rangle|^2 = 0.42$  and  $|\langle 2g|\Phi\rangle|^2 = 0.05$  for the probability of finding respectively  $n = 0.2$  virtual photons in the ground state

| $\Omega_{p/s}^{\max}$ | $T_W$                 | $\tau$                  | $1/\kappa$ | $\gamma$ | $\epsilon$         | $\epsilon'$         | $T$                             |
|-----------------------|-----------------------|-------------------------|------------|----------|--------------------|---------------------|---------------------------------|
| $\Omega_0$            | $\frac{15}{\Omega_0}$ | $\frac{10.5}{\Omega_0}$ | $5T_W$     | $\kappa$ | $\hbar\omega_c$    | $5.9\hbar\omega_c$  | $\frac{\hbar\omega_c}{1.95k_B}$ |
| $50 \times 2\pi$      | 48                    | 33.6                    | 240        |          | $2.03 \times 2\pi$ | $11.98 \times 2\pi$ | 50                              |
| MHz                   | ns                    | ns                      | ns         |          | GHz                | GHz                 | mK                              |

$$\begin{aligned} \mathcal{L}_\gamma = & \gamma_{0\Phi} \mathcal{D}[|0u\rangle\langle\Phi|] + \gamma_{0\Phi} e^{-\beta\epsilon'} \mathcal{D}[|\Phi\rangle\langle 0u|] \\ & + \gamma_{2\Phi} \mathcal{D}[|2u\rangle\langle\Phi|] + \gamma_{2\Phi} e^{-\beta(\epsilon' - 2\omega_c)} \mathcal{D}[|\Phi\rangle\langle 2u|]. \end{aligned} \quad (7)$$

### 3 Results and conclusions

The main result of this work is shown in Fig. 2a where we plot population histories at finite  $T = 50$  mK for an always-on detector, i.e., taking  $\kappa$  constant in our equations. Having in mind repeating the cycle over and over in order to collect a large enough signal for detection, we show a cycle starting from the thermal state of the system (horizontal dashed lines) that for the parameters chosen also ends in the same state, being thus a limiting cycle. Thermal effects reduce the net population transferred, thus the system converts pairs of VPs with a smaller probability. The backaction of the always-on detector is expected to further reduce population transfer and VP conversion due to dephasing during adiabatic passage in STIRAP and to decay of the mode when  $|2u\rangle$  starts to be populated. The former effect leads to a reduction of the final population of  $|2u\rangle$  after the completion of STIRAP estimated by  $P_2 = \frac{1}{3} + \frac{2}{3}\exp[-3\kappa_\phi T^2/(16\tau)]$  [43] where in our case  $\kappa_\phi = 3\kappa/2$  [24], which for the value of  $\kappa$  in Table 1 turns out to be small. On the contrary, decay of the mode after the adiabatic passage phases has a significant impact on ideal STIRAP since it determines in a strong reduction of  $P_2$  (see Fig. 2a). However, this population loss results in the detection of converted VPs photon pairs which progressively populate  $|2u\rangle$  during STIRAP thus the probability of detecting a photon pair per cycle remains large. Notice that the total number of photons decaying in the transmission line (black dotted line in Fig. 2a) is larger than two and increases linearly at very short and large times. This linear component is due to the constant current of thermal photons  $\kappa\langle a^\dagger a \rangle_{th}$  which has nothing to do with VPs. By subtracting the thermal part, we obtain the number of detected VP pairs, which turns out to be almost equal to the thermal population of the initial state  $|0u\rangle$  (gray dotted line in Fig. 2a).

Comparing the continuous measurement of Fig. 2a with the switchable probe protocol of Fig. 1b, we notice that photodetection during the protocol strongly modifies population histories. However, coherent amplification of the VP is preserved since the population of

$|2u\rangle$  decaying before the completion of STIRAP is also due to converted VPs which are being detected. Besides being much simpler to implement, the continuous measurement scheme is faster (notice the time scales in Figs. 2a and 1b) lowering the relative contribution of the stray thermal current. This is apparent in Fig. 2b where we plot for each cycle after thermalization the instantaneous photon current (blue dotted) and the averaged total (blue) and thermal (orange) currents which are proportional to the power respectively emitted into the transmission line. Their difference is the signal due to the converted VPs, which is related to the gray dotted line in Fig. 2a. Summing up, for the continuous measurement scheme, the tradeoff between efficient measurement and decoherence is positive, yielding a sufficiently large extra output power from converted VPs.

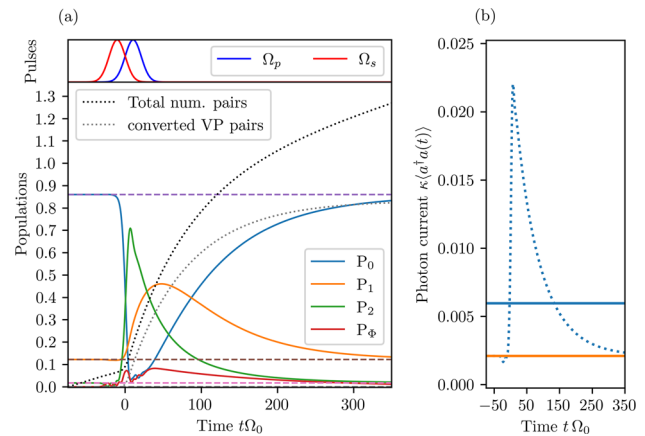


**Fig. 2** **a** A cycle of integrated conversion/photodetection protocol at finite temperatures. The meter is always on, i.e.,  $\kappa \neq 0$  (not represented) is independent on time, allowing for an overall time  $t_M$  shorter than in Fig. 1 (here  $\Omega_0 t_f = 350$ ). Parameters are given in Table 1 and for the case study considered  $t_M = 425/\Omega_0 = 1.36 \mu\text{s}$ . The black dotted line is the total number of photons decaying in the transmission line: it becomes larger than two because of the thermal contribution which is linear in  $t$ . By subtracting it, we obtain the number of converted VPs (gray dotted line). The four horizontal dashed lines are the thermal populations. **b** The instantaneous emitted current (dotted line) and its average per cycle (blue solid) compared to the thermal current (orange)



We briefly comment on the role of atomic decay. Figure 2a shows that in the integrated protocol, some population appears in  $|\Phi\rangle$  before the completion of STIRAP since the pump pulse repumps to  $|\Phi\rangle$  population which just decayed in  $|0u\rangle$  because of the always-on coupling to the meter. In the absence of atomic decay, this population would remain trapped in  $|\Phi\rangle$  after the completion of STIRAP. If  $\gamma \neq 0$ , this population relaxes non-radiatively to  $|0u\rangle$ , resetting efficiently the system for the next cycle.

In Ref. [24], it has been estimated that a signal corresponding to the case study of Table 1a could be amplified by standard HEMT circuitry and discriminated from thermal noise, this task requiring hundreds of repetitions of the conversion/measurement cycle, which is a reasonable figure. In this work, we have analyzed in detail the dynamics of the continuous measurement, showing that STIRAP is resilient to measurement backaction. It is likely that combining optimal control theory and advanced computational methods of data analysis [31, 44] yields even better figures. For instance, Fig. 2b suggests that shortening the after-STIRAP part of the protocol yields a larger average output power for the converted VPs, while the thermal floor is unchanged. However, the steady-state population of  $|0u\rangle$  may be smaller and that population of the intermediate state may trigger leakage from the four-level subspace, requiring an analysis which takes into account the multilevel nature of the setup proposed in Ref. [24] and the subtleties of the physics of an open system in the USC regime.

**Acknowledgements** We acknowledge J. Rajendran and A. Ridolfo who helped to develop our insight for this paper. This work was supported by the QuantERA grant SiUCs (Grant No. 731473), by the PNRR MUR project PE0000023-NQSTI, by ICSC–Centro Nazionale di Ricerca in High-Performance Computing, Big Data and Quantum Computing, by the University of Catania, Piano Incentivi Ricerca di Ateneo 2020–22, project Q-ICT. EP acknowledges the COST Action CA 21144 superqumap and GSP acknowledges financial support from the Academy of Finland under the Finnish Center of Excellence in Quantum Technology QTF (projects 312296, 336810, 352927,352925).

**Funding** Open access funding provided by Università degli Studi di Catania within the CRUI-CARE Agreement.

**Data Availability** The datasets generated during and/or analyzed during the current study are available from the corresponding author on reasonable request.

**Open Access** This article is licensed under a Creative Commons Attribution 4.0 International License, which permits use, sharing, adaptation, distribution and reproduction in any medium or format, as long as you give appropriate credit to the original author(s) and the source, provide a link to the Creative Commons licence, and indicate if changes were made. The images or other third party material in this article are included in the article's Creative Commons licence, unless indicated otherwise in a credit line to the material. If material is not included in the article's Creative

Commons licence and your intended use is not permitted by statutory regulation or exceeds the permitted use, you will need to obtain permission directly from the copyright holder. To view a copy of this licence, visit <http://creativecommons.org/licenses/by/4.0/>.

## References

1. C. Ciuti, G. Bastard, I. Carusotto, Quantum vacuum properties of the intersubband cavity polariton field. *Phys. Rev. B* **72**, 115303 (2005). <https://doi.org/10.1103/PhysRevB.72.115303>
2. P. Forn-Díaz et al., Ultrastrong coupling regime of light-matter interaction. *Rev. Mod. Phys.* **91**, 025005 (2019)
3. A. Kockum et al., Ultrastrong coupling between light and matter. *Nat. Rev. Phys.* **1**, 19–40 (2019)
4. A. Le Boité, Theoretical methods for ultrastrong light-matter interactions. *Adv. Quantum Technol.* **3**(7), 1900140 (2020). <https://doi.org/10.1002/qute.201900140>
5. A.A. Anappara et al., Signatures of the ultrastrong light-matter coupling regime. *Phys. Rev. B* **79**, 201303 (2009). <https://doi.org/10.1103/PhysRevB.79.201303>
6. G. Günter et al., Sub-cycle switch-on of ultrastrong light-matter interaction. *Nature* **458**, 178–181 (2009). <https://doi.org/10.1038/nature07838>
7. G. Scalari et al., Ultrastrong coupling of the cyclotron transition of a 2D electron gas to a THz metamaterial. *Science* **335**, 1323–1326 (2012)
8. T. Niemczyk et al., Circuit quantum electrodynamics in the ultrastrong-coupling regime. *Nat. Phys.* **6**, 772–776 (2010). <https://doi.org/10.1038/nphys1730>
9. P. Forn-Díaz et al., Observation of the Bloch–Siegert shift in a qubit-oscillator system in the ultrastrong coupling regime. *Phys. Rev. Lett.* **105**, 237001 (2010). <https://doi.org/10.1103/PhysRevLett.105.237001>
10. L. Magazzù et al., Probing the strongly driven spin-boson model in a superconducting quantum circuit. *Nat. Commun.* **9**, 1403 (2018). <https://doi.org/10.1038/s41467-018-03626-w>
11. S. Haroche, J.-M. Raimond, *Exploring the quantum: atoms, cavities and photons* (Oxford University Press, Oxford, 2006)
12. A. Wallraff et al., Strong coupling of a single photon to a superconducting qubit using circuit quantum electrodynamics. *Nature* **421**, 162–167 (2004). <https://doi.org/10.1038/nature02851>
13. I. Rabi, Space quantization in a gyrating magnetic field. *Phys. Rev.* **51**, 652–654 (1937). <https://doi.org/10.1103/PhysRev.51.652>
14. D. Braak, Integrability of the Rabi model. *Phys. Rev. Lett.* **107**, 100401 (2011)
15. O. Di Stefano et al., Photodetection probability in quantum systems with arbitrarily strong light-matter interaction. *Sci. Rep.* **8**(1), 17825 (2018). <https://doi.org/10.1038/s41598-018-36056-1>
16. C. Ciuti, I. Carusotto, Input-output theory of cavities in the ultrastrong coupling regime: the case of time-independent cavity parameters. *Phys. Rev. A* **74**, 033811 (2006). <https://doi.org/10.1103/PhysRevA.74.033811>

17. S. De Liberato, C. Ciuti, I. Carusotto, Quantum vacuum radiation spectra from a semiconductor microcavity with a time-modulated vacuum Rabi frequency. *Phys. Rev. Lett.* **98**, 103602 (2007). <https://doi.org/10.1103/PhysRevLett.98.103602>
18. S. De Liberato et al., Extracavity quantum vacuum radiation from a single qubit. *Phys. Rev. A* **80**, 053810 (2009). <https://doi.org/10.1103/PhysRevA.80.053810>
19. R. Stassi et al., Spontaneous conversion from virtual to real photons in the ultrastrong-coupling regime. *Phys. Rev. Lett.* **110**, 243601 (2013). <https://doi.org/10.1103/PhysRevLett.110.243601>
20. J.-F. Huang, C.K. Law, Photon emission via vacuum-dressed intermediate states under ultrastrong coupling. *Phys. Rev. A* **89**, 033827 (2014). <https://doi.org/10.1103/PhysRevA.89.033827>
21. G. Falci et al., Advances in quantum control of three-level superconducting circuit architectures. *Fort. Phys.* **65**, 1600077 (2017). <https://doi.org/10.1002/prop.201600077>
22. O. Di Stefano et al., Feynman-diagrams approach to the quantum Rabi model for ultrastrong cavity QED: stimulated emission and reabsorption of virtual particles dressing a physical excitation. *New J. Phys.* **19**(5), 053010 (2017). <https://doi.org/10.1088/1367-2630/aa6cd7>
23. G. Falci et al., Ultrastrong coupling probed by coherent population transfer. *Sci. Rep.* **9**, 9249 (2019). <https://doi.org/10.1038/s41598-019-45187-y>
24. L. Giannelli et al. “Detecting virtual photons in ultrastrongly coupled superconducting quantum circuits”. [arXiv:2302.10973](https://arxiv.org/abs/2302.10973) (2023)
25. T.M. Hazard et al., Nanowire superinductance fluxonium qubit. *Phys. Rev. Lett.* **122**, 010504 (2019)
26. M. Peruzzo et al., Surpassing the resistance quantum with a geometric superinductor. *Phys. Rev. Appl.* **14**, 044055 (2020). <https://doi.org/10.1103/PhysRevApplied.14.044055>
27. W. Zhang et al., Microresonators fabricated from high-kinetic-inductance aluminum films. *Phys. Rev. Appl.* **11**, 011003 (2019). <https://doi.org/10.1103/PhysRevApplied.11.011003>
28. P.G. Di Stefano et al., Nonequilibrium thermodynamics of continuously measured quantum systems: a circuit QED implementation. *Phys. Rev. B* **98**, 144514 (2018). <https://doi.org/10.1103/PhysRevB.98.144514>
29. N.V. Vitanov et al., Stimulated Raman adiabatic passage in physics, chemistry, and beyond. *Rev. Mod. Phys.* **89**, 015006 (2017). <https://doi.org/10.1103/RevModPhys.89.015006>
30. N. Vitanov et al., Coherent manipulation of atoms and molecules by sequential laser pulses. *Adv. At. Mol. Opt. Phys.* **46**, 55–190 (2001). [https://doi.org/10.1016/S1049-250X\(01\)80063-X](https://doi.org/10.1016/S1049-250X(01)80063-X)
31. L. Giannelli et al., A tutorial on optimal control and reinforcement learning methods for quantum technologies. *Phys. Lett. A* **434**, 128054 (2022). <https://doi.org/10.1016/j.physleta.2022.128054>
32. K. Bergmann, H. Theuer, B. Shore, Coherent population transfer among quantum states of atoms and molecules. *Rev. Mod. Phys.* **70**(3), 1003–1025 (1998). <https://doi.org/10.1103/RevModPhys.70.1003>
33. G. Falci et al., Design of a Lambda system for population transfer in superconducting nanocircuits. *Phys. Rev. B* **87**, 214515–1–214515–13 (2013). <https://doi.org/10.1103/PhysRevB.87.214515>
34. P.G. Di Stefano et al., Population transfer in a Lambda system induced by detunings. *Phys. Rev. B* **91**, 224506 (2015). <https://doi.org/10.1103/PhysRevB.91.224506>
35. P.G. Di Stefano et al., Coherent manipulation of noise-protected superconducting artificial atoms in the Lambda scheme. *Phys. Rev. A* **93**, 051801 (2016). <https://doi.org/10.1103/PhysRevA.93.051801>
36. A. Vepsäläinen et al., Quantum control in qutrit systems using hybrid Rabi-STIRAP pulses. *Photonics* **3**, 62 (2016). <https://doi.org/10.3390/photonics3040062>
37. K. Kumar et al., Stimulated Raman adiabatic passage in a three-level superconducting circuit. *Nat. Commun.* **7**, 10628 (2016). <https://doi.org/10.1038/ncomms10628>
38. H. Xu et al., Coherent population transfer between uncoupled or weakly coupled states in ladder-type superconducting qutrits. *Nat. Commun.* **7**, 11018 (2016). <https://doi.org/10.1038/ncomms11018>
39. A. Ridolfo et al., Probing ultrastrong light-matter coupling in open quantum systems. *Eur. Phys. J. Spec. Top.* **230**, 941–945 (2021)
40. C. Eichler et al., Experimental state tomography of itinerant single microwave photons. *Phys. Rev. Lett.* **106**, 220503 (2011). <https://doi.org/10.1103/PhysRevLett.106.220503>
41. J.C. Curtis et al., Single-shot number-resolved detection of microwave photons with error mitigation. *Phys. Rev. A* **103**, 023705 (2021). <https://doi.org/10.1103/PhysRevA.103.023705>
42. B. Spagnolo et al., Relaxation phenomena in classical and quantum systems. *Acta Phys. Pol B* (2012)
43. P.A. Ivanov, N. Vitanov, K. Bergmann, Effect of dephasing on stimulated Raman adiabatic passage. *Phys. Rev. A* **70**, 063409 (2004). <https://doi.org/10.1103/PhysRevA.70.063409>
44. J. Brown et al., Reinforcement learning-enhanced protocols for coherent population transfer in three-level quantum systems. *New J. Phys.* **23**(9), 093035 (2021)